FEATURE ARTICLE

physica
**pss**
status
solidi
b

www.pss-b.com

# Surface Stress and Lattice Dynamics in Oxide Ultrathin Films

*Jörg Premper, Florian O. Schumann, Anita Dhaka, Sebastian Polzin, Krassimir L. Kostov, Veronica Goian, Dirk Sander, and Wolf Widdra\**

The lattice misfit between the substrate and an epitaxial film leads in general to static forces, which define the interface stress, and dynamic responses that modify the thin-film lattice dynamics. Although these are both fundamental concepts that are important for film growth and thin-film properties, they have not been investigated in a combined way so far. Therefore, herein, surface stress experiments in combination with surface phonon studies for three different, cubic oxide ultrathin film systems are reviewed. Within the class of binary oxides, NiO(001) grown on Ag(001) is chosen, which exhibits a −2.2% lattice mismatch, and BaO(001) on Pt(001), a system with a negligible lattice mismatch. For the ternary oxides, perovskite thin films of $BaTiO_3$ grown epitaxially on Pt(001) with a lattice mismatch of −2.3% are focused upon. The surface stress experiments are conducted with an optical two-beam curvature technique under in situ growth conditions. Surface and thin-film phonons are determined by high-resolution electron energy loss spectroscopy. Surface stress and lattice dynamics are discussed in the range from the oxide monolayer to thin films of about 20 unit cell in thickness.

## 1. Introduction

Mechanical stress may appear at interfaces of thin oxide films due to a modified local bonding to the substrate below or the layer above as compared with a bulk-like situation or due to strain from a lattice mismatch between the substrate and oxide thin film. The appearance of interface or surface stress can be related to modified electronic, magnetic, and lattice dynamics properties if they deviate from the respective bulk properties. Whereas the relation of lattice strain and oxide thin-film properties has attracted strong attention for tuning specific properties,[1,2] much less is know for thin-film stress.

For the epitaxial growth of oxide thin films, the lattice mismatch between the substrate and the film defines the thin-film

strain and is essential for mechanical stress in the film. While for thick films a description of the strain–stress interrelation based on bulk elastic properties may be sufficient, the situation is likely to change for ultrathin films of only a few unit cells thickness, where one may expect significantly altered elastic properties. At the microscopic level, the elastic properties originate from the sum of interatomic forces that are also governing the specific lattice dynamics that defines the thin-film phonons. Interface stress and lattice dynamics may be seen as the static and dynamic response on external mechanical stimuli.

Here we join experimental data on the lattice dynamics and lattice stress in ultrathin oxide films grown on metal substrates. Our study is based on in situ stress measurements which include the film stress-induced curvature of a thin-film-substrate composite with submonolayer sensitivity and an accuracy in the 5% range. In short, the measurement of the film or surface stress-induced curvature change allows to extract film and interface stress changes quantitatively. This setup has been used successfully to monitor surface stress changes upon adsorption and surface reconstruction, to measure film stress during monolayer film growth and magnetization processes.[3–6] Thus, in combination with complementary techniques such as low-energy electron diffraction (LEED) and surface x-ray diffraction, quantitative insights into the correlation between film growth, interfacial atomic structure, lattice strain, and magnetoelastic coupling on the atomic scale were obtained. In the present work, we combine the stress measurement with inelastic electron scattering to determine the surface phonons of ultrathin films and their film

Dr. J. Premper, Dr. A. Dhaka, Dr. D. Sander, Prof. W. Widdra
Max-Planck-Institut für Mikrostrukturphysik
D-06120 Halle, Germany
E-mail: wolf.widdra@physik.uni-halle.de

Dr. F. O. Schumann, S. Polzin, Prof. W. Widdra
Institute of Physics
Martin-Luther-Universität Halle-Wittenberg
D-06099 Halle, Germany

Prof. K. L. Kostov
Institute of General and Inorganic Chemistry
Bulgarian Academy of Sciences
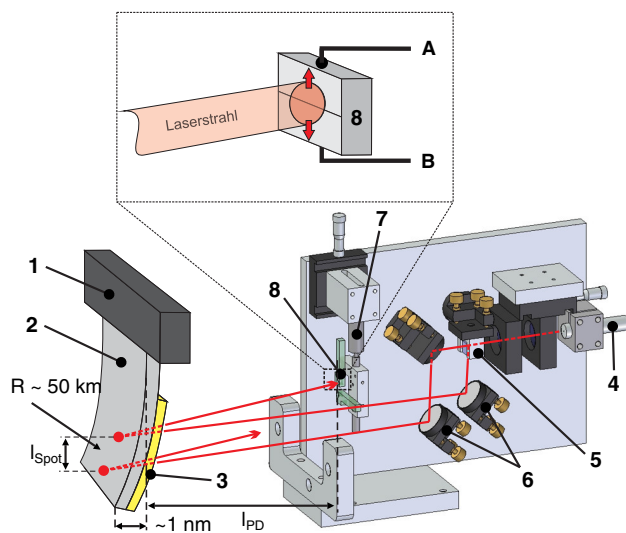1113 Sofia, Bulgaria

Dr. V. Goian
Institute of Physics
The Czech Academy of Sciences
182 21 Prague, Czech Republic

thickness dependence. It combines both aspects in a truly complementary manner beyond work reported so far and can provide insights into the correlation between stress and lattice dynamics in oxide films. A better understanding of the underlying physics is mandatory for a deeper understanding of the largely unresolved interplay between atomic structure, mechanical stress, and lattice dynamics at interfaces and in atomic layer thin oxide films.

## 2. Experimental Section

Mechanical stress at surfaces, interfaces, and in films can be measured quantitatively by exploiting the stress-induced curvature of a thin substrate. **Figure 1** shows a schematic of stress measurement. A thin rectangular substrate was clamped along its width at one end, whereas the other end was free. Stress during film growth on the front surface of a such a cantilevered substrate induced a minute change of curvature of the substrate, and the precise measurement of this curvature change provided quantitative access to stress. The underlying principles have been reviewed in depth,[3,8–11] and here we focus on a particular aspect which makes stress measurements during oxide film growth an experimentally challenging endeavor.

The measurement of mechanical stress during growth of the atomic layer thin oxide films presents experimental challenges which are linked to two specific experimental conditions: 1) oxygen partial pressure during growth and 2) a high temperature during oxide film growth. The experimental challenge was caused by the corresponding oxidation process which was not limited to the film but also affected the sample holder and its components. These oxidation processes are more pronounced

**Dirk Sander** received his Ph.D. from RWTH Aachen, Germany, in 1992. He worked at IBM T.J. Watson Research Center, Yorktown Heights, New York, USA for 1 year before he joined the newly founded Max Planck Institute of Microstructure Physics, Halle(Saale), Germany, in 1993. He received his Habilitation from Martin-Luther-Universität Halle-Wittenberg in 1999. He worked several months as a visiting professor at the University Aix-Marseille, France. His research interests include stress at interfaces and in atomic layers, magnetism on the nanoscale, and spin-dependent electronic properties of surfaces. He is recipient of the Gaede Prize of the German Vacuum Society.
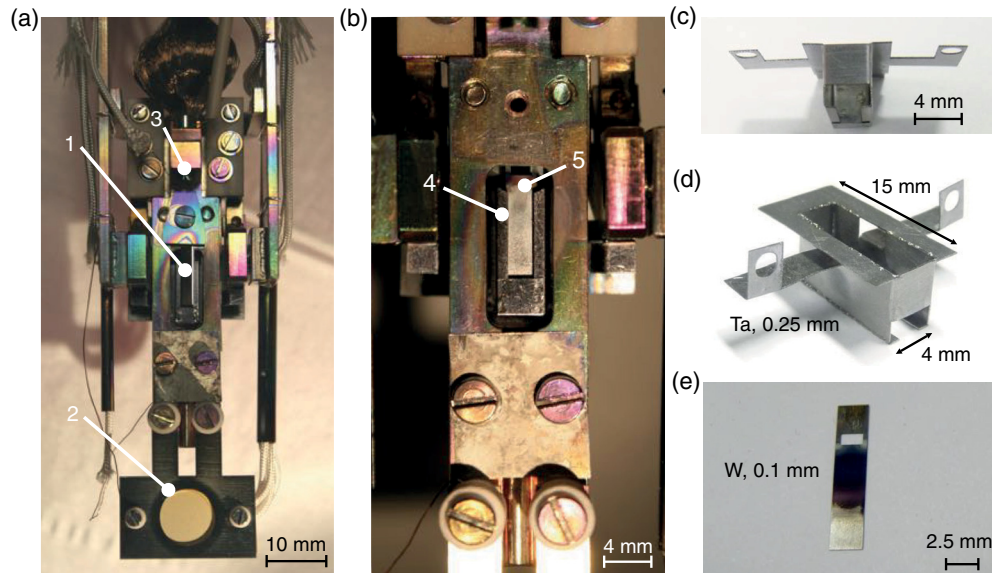
**Wolf Widdra** received his Ph.D. in physics in 1991 at the Philipps-Universität Marburg, Germany. After a postdoc at UC Santa Barbara, USA, he became an assistant professor in the group of Dietrich Menzel at the TU Munich, Germany, in 1994. From 2001 to 2003, he worked as an associate professor at the TU Berlin and headed the Department "Synchrotron Radiation, Micro- and Nanostructures at the Max Born Institute for Nonlinear Optics and Short Pulse Spectroscopy" in Berlin. Since 2003, he has been full professor at the Martin-Luther-Universität Halle-Wittenberg as head of the surface science department.

at a high temperature. The oxidation processes of sample holder components constituted a severe problem, as the curvature measurement was sensitive to the smallest variation of the sample slope and sample deflection, where deflection on the nm scale of the cantilever sample was detected. An oxidation of the sample holder, with the corresponding dimensional change in components, inevitably led to a deflection of the sample. Figure 1 shows that two optical beams were used to measure the sample curvature directly from the difference of sample slope at two positions. This setup proved to be very robust for room-temperature stress measurements, even in the presence of oxidizing agents in the ultrahigh vacuum chamber. Stress measurements during monolayer thin oxide growth were carried out successfully.[12,13]

Stress measurements at a high sample temperature of order 900 K and in an oxygen atmosphere required further specific experimental modifications of the sample holder to ensure reliable quantitative stress measurements, as shown in **Figure 2**. These modifications aim at providing a high temperature stability of all components by thermal shielding, and they ensure that oxidation processes do not impact the sample clamping and its support in an undue manner. Figure 2 shows the sample holder which we conceived, designed, built, and used successfully for high-temperature stress measurements in an oxidizing atmosphere during the pulsed laser deposition (PLD) of perovskite oxides onto single-crystal sample surfaces.[7,14,15]



**Figure 1.** A schematic of the two-beam stress-induced curvature measurement. 1: sample holder, 2: sample, 3: deposited film on the sample surface, 4: laser diode with beam forming optics, 5: 1:1 beam splitter, 6: mirror on tilt mount, 7: piezotranslator stage, 8: split-photodiode. Inset: split photodiode with photocurrent leads A and B. The sample deflection is largely exaggerated, it amounts to 1 nm for a stress of 1 GPa, then the radius of curvature $R$ is of the order 50 km. The split photodiode is positioned at a distance of $l_{PD} = 280$ mm away from the sample, the two laser beams hit the sample at a vertical distance of $l_{Spot} = 5$ mm.

**Figure 2.** Details of the sample holder used for high-temperature stress measurements. a) 1: single-crystal sample, 2: quartz oscillator, 3: sample holder. b) 4: Ta cage surrounding W filament (not visible), 5: W radiation shield (sample removed). c) Ta cage surrounding W filament, viewed from the front, Ta strips with holes not bent. d) Ta cage surrounding W filament with mounting strip bent. e) Zoom in: W radiation shield with cutout to reduce thermal loss to sample holder. Adapted with permission.[14] Copyright 2015, Elsevier (see also ref. [7]).

Phonons within the ultrathin oxide films were measured by high-resolution electron energy loss spectroscopy (HREELS)[16–18] with a Delta05 high-resolution spectrometer (SPECS, Berlin). It offered an energy resolution down to 5.7 cm$^{-1}$ at an intensity of the specularly reflected beam of $10^5$ s$^{-1}$ for the Ru(001) surface. The vibrational spectra presented here for oxide thin films were measured with a resolution of about 16–20 cm$^{-1}$. In all HREELS experiments the oxide thin films were grown in situ by molecular beam epitaxy (MBE) with subsequent annealing.

## 3. Binary Oxide Thin Films

Many binary oxides in which the metal cation possesses a bivalent oxidation state grow in the NaCl rocksalt structure. Examples are MgO, NiO, CoO, MnO, and BaO. All of them have been grown epitaxially on appropriate metal substrates, mostly in (001) orientation but also in (111) and (110) phases.[19–23] In the present work we restrict ourselves to the two examples of BaO(001) on Pt(001) and NiO(001) on Ag(001). The former exhibits a nearly vanishing lattice misfit, whereas NiO(001)/Ag(001) has a lattice misfit of about −2.2%.

### 3.1. Barium Oxide

In contrast to many other oxides with rocksalt structure, there are only a few investigations of the thin-film properties of BaO, despite its application as catalyst for the control of NO$x$ emission or as a buffer layer for epitaxial perovskite oxide growth.[24,25] The lattice dynamics of bulk BaO is reported in several earlier studies.[26,27] However, our study is the first work related to the vibrational properties of BaO thin films.[28] The experimental challenge arises from the high reactivity of Ba which renders stabilization of a pure BaO phase difficult in thin films and bulk samples.[27] We grow BaO(001) ultrathin films by Ba deposition from commercial getter sources (SAES Getters, Milan, Italy) on a Pt(001) single crystal at 300 K. BaO films were formed by subsequent annealing in an oxygen atmosphere of $10^{-6}$ mbar. We observe epitaxial long-range ordered BaO(001)-(1 × 1) thin films with a film rotation of 45° with respect to the substrate. This leads to a nearly unstrained growth where the smallest possible BaO(001)-(1 × 1) unit cell matches a Pt(001)-c(2 × 2) substrate cell.

For the unstrained growth, we expect three degenerated transversal optical (TO) modes for the BaO thin film. HREEL spectra for a 25 ML BaO(001)-(1 × 1) film are shown in **Figure 3**a for different annealing temperatures. The improved long-range order upon annealing becomes immediately visible by the increased intensity of the vibrational energy loss at about 400 cm$^{-1}$. The diffraction pattern of a similarly annealed film of 20 ML is shown in Figure 3c and shows a sharp c(2 × 2) structure relative to the Pt(001) substrate, which corresponds to the unreconstructed BaO(001)-(1 × 1). Details of the vibrational spectrum together with a scattering calculation based on a one-oscillator model (red line) are shown in Figure 3b. The excitation of the Fuchs–Kliewer (FK) surface phonon polariton,[29] as well as its double and triple loss, dominates the spectrum. The relationship between the FK frequency $\omega_{FK}$ and the bulk TO mode is given for an infinite thick film by

$$\hbar\omega_{FK} = \sqrt{\frac{\varepsilon_0 + 1}{\varepsilon_\infty + 1}}\hbar\omega_{TO} \tag{1}$$

where $\varepsilon_0$ and $\varepsilon_\infty$ are the static and high-frequency permittivities.[29,30] With the dielectric properties $\varepsilon_0$ and $\varepsilon_\infty$ for bulk BaO and $\omega_{TO}$ from ref. [26], the FK frequency is predicted to 395.3 cm$^{-1}$, in good agreement with 390 cm$^{-1}$ in the 25 ML spectra.
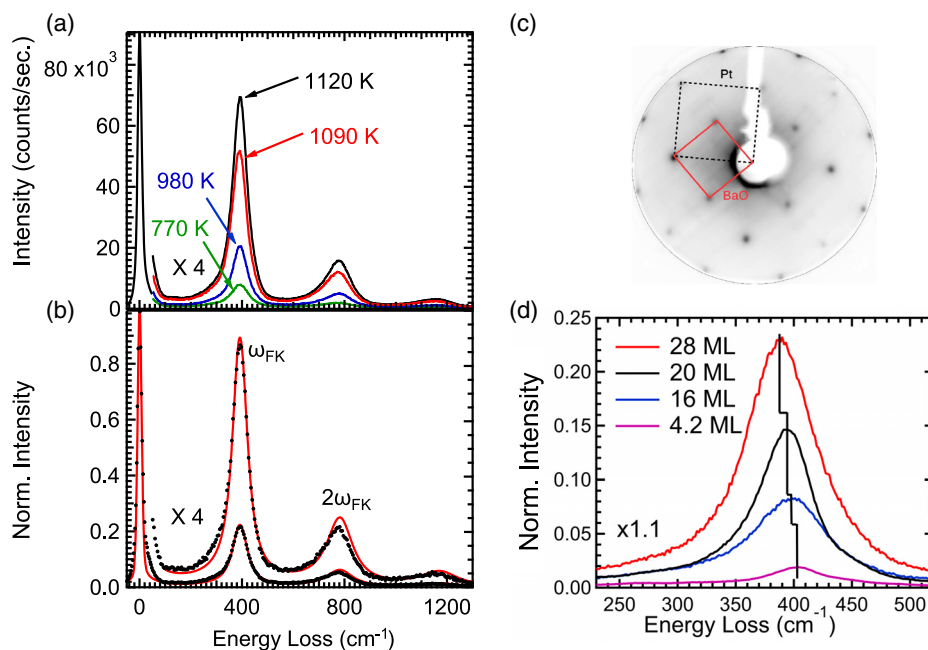
**Figure 3.** BaO(001) thin films on Pt(001): a) HREEL spectra for a 25 ML thin film with increased annealing temperatures (not normalized to the elastic peak). b) A comparison of scattering calculation based on a one-oscillator model (red line) with the spectrum (black markers) upon annealing to 1120 K. c) LEED pattern for 20 ML BaO(001) at a kinetic energy of 80 eV. d) HREEL spectra for film thickness from 4 to 28 ML. Adapted with permission.[28] Copyright 2018, IOP Publishing Ltd.

Although the BaO films grow unstrained as based on the BaO and Pt lattice constants, the spectra for BaO films of different thicknesses reveal a systematic shift of the FK frequency with film thicknesses, as shown in Figure 3d. This shift is shown in **Figure 4**a for thicknesses from 2 to 28 ML.[28] The intensity of the phonon increases, as shown in Figure 4b with film thickness. The dominant contribution to the frequency shift comes from the modification of the effective dielectric response. For thick films the response converges to the dielectric properties of bulk BaO, whereas for thinner films the contribution from the metal substrate grows. As described in a previous study[28] in detail, this combined response leads to a continuos downshift of the FK frequency with increasing film thickness which converges to a BaO bulk value of 382 cm$^{-1}$, as shown by a red solid line in Figure 4a. It well describes the shift for thin films >10 ML. However for thinner films the standing wave character of the TO phonon perpendicular to the thin film has to be taken into account. As shown in Figure 4c, the longest allowed wavelength within a film of thickness $d$ is $\lambda = 2d$. The standing wave character shifts the optical mode from the zone-center wavevector $q = 0$ to a finite $q = \pi/d$, as shown in Figure 4d. In the presence of a substantial longitudinal optical (LO) phonon dispersion along the [001] direction, it leads to a frequency downshift. Consequently, the FK phonon will experience a downshift (open red circles) in Figure 4a.[28] In summary for the unstrained BaO thin films on Pt(001), we find a shift of the FK surface phonon polariton for BaO thin films that can be fully described by dielectric theory using the BaO bulk dielectric properties and the bulk phonon dispersion, when a standing-wave correction is applied. In the following sections, we will compare the unstrained case of BaO with strained growth of NiO.

## 3.2. Nickel Oxide

### 3.2.1. Surface Stress

Numerous studies have been conducted in the past to investigate growth and structure of NiO on Ag(001), and our studies provide quantitative data on stress and lattice dynamics.[12,13,31,32] The seemingly simple system NiO on Ag(001) is characterized by a compressive epitaxial misfit of $\eta = -0.022$ ($\eta = (a_{NiO} - a_{Ag})/a_{Ag}$, $a_{Ag} = 4.086$ Å, $a_{NiO} = 4.177$ Å). Its growth is characterized by a complex interface formation,[33–35] which gives rise to a nontrivial stress evolution with NiO thickness, as shown in **Figure 5**. From the formation of a NiO bilayer, the stress change drops by about 7 N m$^{-1}$ until a thickness of 5–6 ML is reached. As evidenced by the medium-energy electron diffraction (MEED) oscillations shown as blue markers in Figure 5, the growth proceeds in a layer-by-layer mode. This growth mode continues up to 15 ML. However, beyond 5 ML NiO thickness a gradual transition to nonpseudomorphic growth with bulk-like NiO is observed by stress and LEED measurements.[31] For the first monolayer the combination of stress measurements with surface x-ray diffraction and density functional theory reveals that the interface between NiO and Ag is more complex than anticipated[12] and is not discussed here. It is characterized by a direct O–Ag interaction and by embedded NiO patches in the surface of Ag, giving rise to a small tensile interface stress, which contrasts with the compressive misfit between NiO and Ag. A compressive film stress in quantitative agreement with the lattice misfit is measured in films thicker than 2 ML that will be compared with phonon data in the last section.
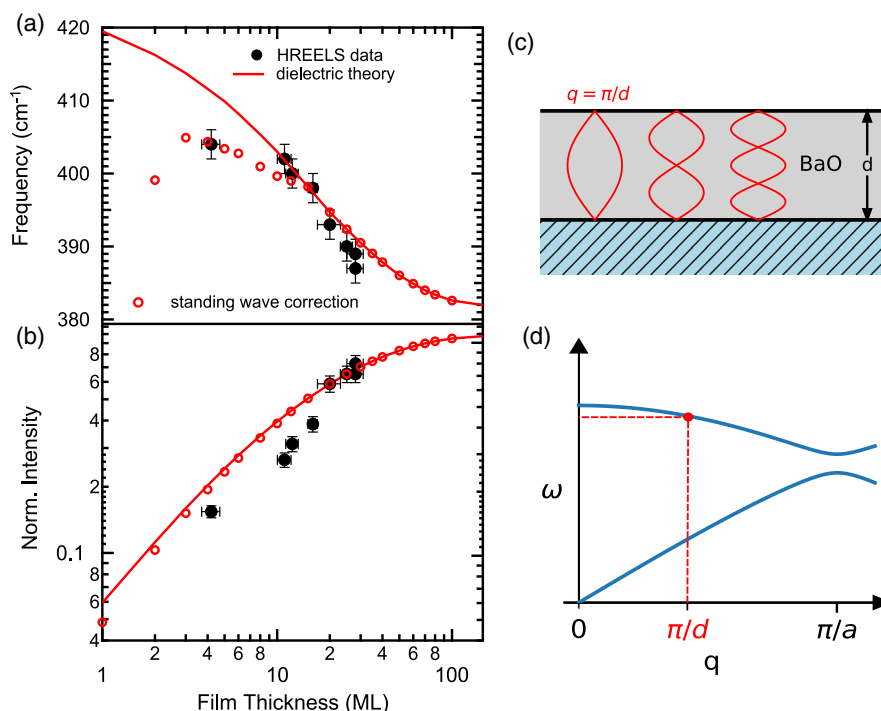
**Figure 4.** BaO(001) thin films on Pt(001): a) Thickness-dependent surface phonon polariton frequency and b) normalized intensity (black symbols). The calculated frequencies and intensities without and with standing-wave corrections are shown as red lines and as red open circles, respectively. c) Schematics of the standing-wave phonon pattern perpendicular to the film with thickness $d$. d) Simplified schematics of the phonon dispersion within a bulk oxide in (001) direction. In a thin film, the longest wavelength $2d$ corresponds to a smallest wavevector $q_{\perp,min}$ perpendicular to the surface that can be realized within the film. The surface loss function is therefore not tested at $q_\perp = 0$ as for infinite thickness, but at a wavevector $q_{\perp,min} = 2d$. Correspondingly, the bulk frequencies $\omega_{TO}(q_{\perp,min})$ and $\omega_{LO}(q_{\perp,min})$ have to be considered, which lead in the cases of BaO and NiO to a downshift of the FK phonon polariton for ultrathin films. Partly adapted from ref. [28] with permission. Copyright 2018, IOP Publishing Ltd.

### 3.2.2. Surface Phonons

HREEL spectra for NiO(001) thin films of various thicknesses as grown by MBE are shown in **Figure 6**a. The NiO monolayer (bottom spectrum) has quite distinct structural and vibrational properties as compared with thicker films, as discussed previously.[31] It forms a uniaxially compressed "$(2 \times n)$" superstructure which relaxes back to a $(1 \times 1)$ structure as soon as the second NiO layer is grown on top.[31,34,35] A similar initial NiO growth is found on other (001)-oriented fcc metal surfaces.[36] Starting from the second ML, we find, besides a microscopic Wallis mode at about $400\,cm^{-1}$ the characteristic FK surface phonon polariton that has been identified as the main energy loss of NiO surfaces and thin films.[37,38] On Ag(001), the FK is upshifting from 440 to $560\,cm^{-1}$ with NiO film thickness.[31,39] This shift is much stronger and has an opposite sign as compared with the structural similar BaO thin-film system discussed earlier. The shift and the intensity increase is shown in Figure 6b,c. The black and blue solid lines in Figure 6b show the results of the dielectric theory without and with the standing-wave correction, similar as discussed earlier for BaO ultrathin films.[31] Clearly the theory as based on NiO bulk properties fails to describe the experimentally observed frequency shift of the FK mode. Note that the Wallis mode as a microscopic mode is by far less thickness dependent and shifts only from 405 to $425\,cm^{-1}$ in the same thickness

range. Its intensity stays constant above 5 ML. The quantitative comparison of the experimental HREELS data with the calculated loss function based on the dielectric theory reveals bulk-like phonon properties for NiO(001) for a thickness above 15 ML. However, for NiO(001) thicknesses from 2 to 5 ML, a strong phonon softening is found that is attributed to the surface stress that results from the lattice mismatch. Note that this thickness range shows the drastic stress changes in Figure 5 where it is marked as orange region II. In the range between 5 and 15 ML that is marked as green region III in Figure 5, the stress starts to relax and at the same time the FK phonon relaxes towards a bulk-phonon-derived frequency. In this region the Wallis mode stays constant in intensity and frequency. As we discuss later, our experiments provide the first reference data for a quantitative comparison of the interrelation between surface stress and phonon softening in binary oxides.

In Figure 6 we have compiled data for the dipole active modes at $q = 0$, which dominate the HREEL spectra under the most frequently used specular scattering conditions. However, the full phonon dispersion is also accessible in off-specular scattering experiments. Such data are shown in **Figure 7**a for a 4 ML NiO(001) film and an electron primary energy of 81 eV (for details, see a previous study[39]). At this primary energy, phonon spectra for $q$ vectors within the first and second surface Brillouin zone can be recorded. The analysis of

ADVANCED
SCIENCE NEWS
www.advancedsciencenews.com

physica
status
solidi b
www.pss-b.com
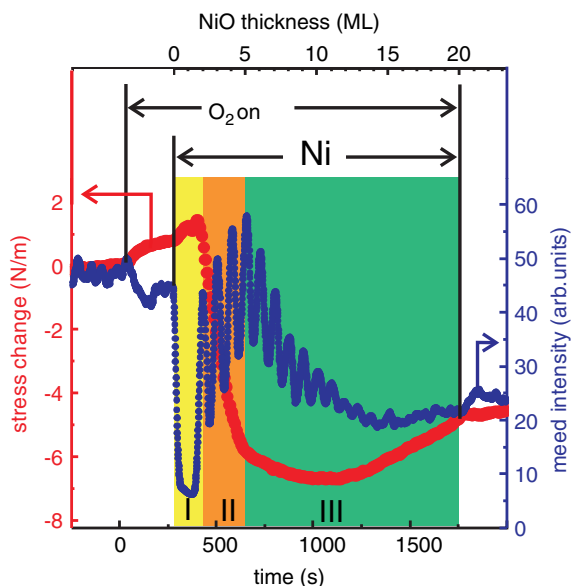
**Figure 5.** Stress change (left axis) and MEED intensity (right axis) during Ni deposition on Ag(001) at 300 K. $p_{O_2}$ : $2 \times 10^{-7}$ mbar. MEED oscillations from 2 to 15 ML indicate layer-by-layer growth, the negative (compressive) stress change form 2–5 ML is ascribed to epitaxial misfit stress. Stress regime I (yellow): interface formation, II (orange): pseudomorphic growth, III (green): non-pseudomorphic growth. Adapted with permission.[12] Copyright 2011, APS (see also ref. [13]).

HREELS data for a wide range of primary energies between 4 and 255 eV is shown in the phonon dispersion plot in Figure 7b by open circles. The projection of the NiO bulk phonon modes as derived from DFT + U frozen phonon

calculations[32] onto the first Brillouin zone is shown by the gray background for comparison. Eight phonon modes with either surface or surface resonance character have been identified, as indicated by colored symbols in Figure 7b. Most prominently, the Rayleigh phonon (light blue symbols) shows a strong dispersion from about 60 cm$^{-1}$ at 0.35 Å$^{-1}$ to 172 cm$^{-1}$ at the $\overline{X}$ point and follows the lower edge of the bulk acoustic modes. All other modes show a weaker dispersion and have a pronounced intensity where they fall into or are close to pockets of the projected bulk density of states, as, e.g., the strong $S_6$ mode at 285 cm$^{-1}$ around $\Delta k_\parallel = 1.07$ Å$^{-1}$ in Figure 7a. These data for the strained NiO thin film can be compared with the surface phonon dispersion for an unstrained NiO(001) film of 25 ML as reported in a previous study[32] and marked in Figure 7b by solid markers. The comparison reveals equivalent dispersion data for a 4 ML thin film as compared with the surface phonon dispersion of NiO(001). Already at 4 ML thickness, the full NiO phonon dispersion is formed and the strained state of the thin film leads only to subtle differences in the microscopic phonon response. Most prominently, we find a red shift of 40 cm$^{-1}$ for the $S_6$ mode (magenta open and solid circles) at the zone center, as well as smaller red shifts for the modes at 340 and 400 cm$^{-1}$ (red and blue circles in Figure 7b, respectively) close to the $\overline{X}$ point.

## 4. Barium Titanate Thin Films

### 4.1. Surface Stress

Epitaxial perovskite oxides such as BaTiO$_3$ (BTO) on Pt(001) have been prepared by PLD in an oxygen atmosphere at an elevated sample temperature of 930 K for the stress
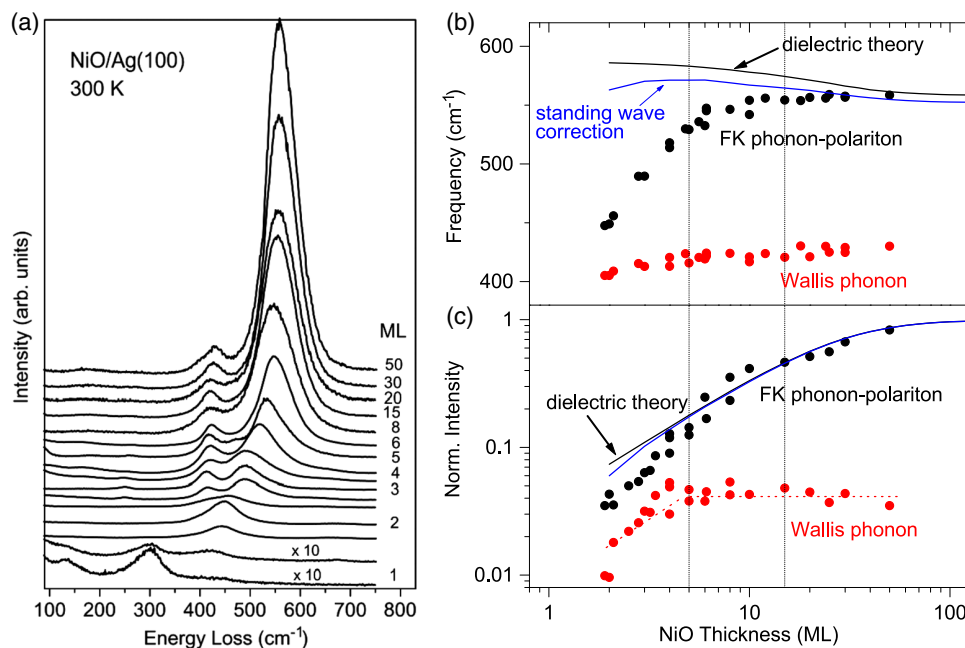


**Figure 6.** a) HREEL spectra for Ni(001) ultrathin films on Ag(001) for various film thicknesses between 1 and 50 ML. b) Thickness-dependent phonon frequency and intensity c) for the FK (black circles) and the Wallis mode (red circles). Calculated shifts based on dielectric theory without and with a standing-wave correction are indicated by black and blue solid lines, respectively. Adapted with permission[31]. Copyright 2016, APS.
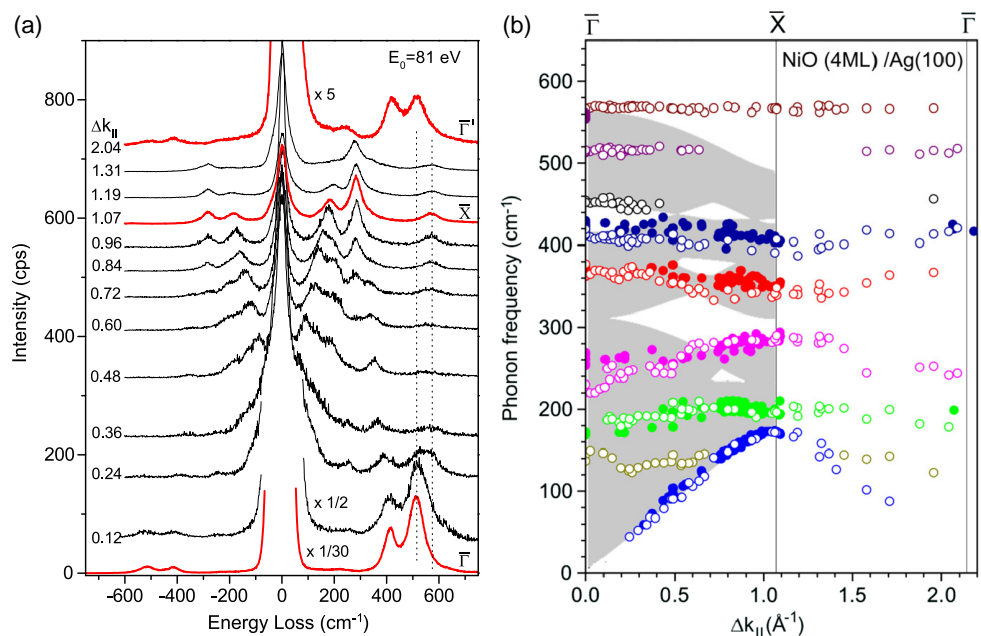
**Figure 7.** Surface phonon dispersion of a 4 ML ultrathin NiO(001) film on Ag(001): a) HREEL spectra for a primary electron energy of 81 eV. The spectra are shifted vertically with increasing scattering angle (increasing momentum transfer $\Delta k_\parallel$ as indicated on the left side). b) Extracted phonon dispersion data from HREELS data for different primary electron energies between 4 and 255 eV (open circles). For comparison, data for a 25 ML-thick (bulk-like) film are shown by solid circles. Bulk NiO phonon modes as derived from DFT + U frozen phonon calculations[32] projected on the first surface Brillouin zone are marked by a gray background. Adapted with permission.[39] Copyright 2016, Elsevier.

measurements. For phonon measurements, the films were prepared by MBE as described in more detail below. LEED measurements were carried out in all cases to obtain a transfer standard to ensure that films of comparable crystalline quality were obtained. In thin films, the epitaxial misfit between BTO and Pt gives rise to a compressive misfit strain of $\eta = -0.023$, which leads to a calculated misfit stress of $-4.0$ GPa based on the bulk elastic data.[7] The stress measurements in conjunction with in situ LEED, as shown in **Figure 8**, indicate a compressive stress in an 18 unit cell (u.c.) thin BTO film of $-4.2$ GPa. The LEED pattern indicates epitaxial growth of BTO with a c-$(2 \times 2)$ surface structure with respect to the Pt(001) substrate. Both results support the conclusion that BTO grows on Pt(001) epitaxially strained with a sizeable compressive stress of order $-4$ GPa. The LEED measurements may serve as a transfer standard to compare films prepared by PLD with those prepared in other labs by MBE. The comparison shows that indeed the deposition methods, PLD and MBE, both give rise to films of a comparable epitaxial order. This is a priori not guaranteed, as both methods differ substantially in the deposition kinetics and deposition environment. Film stress in BTO films is correlated with characteristic changes in the BTO vibrational spectra as compared with bulk BTO, as discussed later.

### 4.2. Surface Phonons

For the HREELS measurements, all BTO ultrathin films have been prepared by in situ MBE using separate Ba and Ti evaporation sources. The large-scale quasihexagonal c(26 × 118)

reconstruction of the bare Pt(001)[40] has been removed by an initial deposition of a monolayer of BaO with subsequent growth of the BaTiO₃ thin film at 300 K. The films have been finally annealed to 900–950 K in $4 \times 10^{-6}$ mbar oxygen. As for PLD growth, we observe a sharp c(2 × 2) LEED pattern with respect to the Pt(001) substrate that corresponds to a BaTiO₃(001)-(1 × 1) structure. For a thin film of four unit cell thickness, the LEED pattern is shown in the inset of **Figure 9**a.
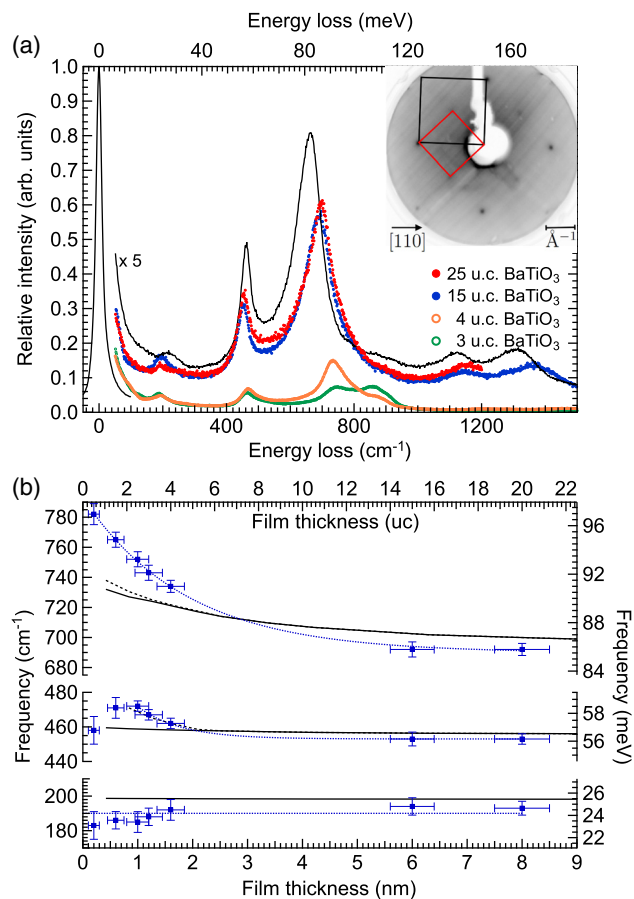
HREEL spectra recorded at room temperature for BTO(001) thin films on Pt(001) in the thickness range between 3 and 25 unit cells are shown in Figure 9 in different colors. The spectrum of a BTO(001) single-crystal surface, which has been prepared by argon ion sputtering and annealing in $4 \times 10^{-6}$ mbar oxygen, is shown by a black solid line for comparison. It can be compared with recent data for the bulk optical properties of BTO, as measured by normal incidence infrared absorption spectroscopy for undoped and slightly doped (001)-oriented single crystals.[41,42] The ferroelectric BTO has three well-known polar and a silent lattice mode, which are modified upon oxygen vacancy doping.[41–44] In addition, a recently characterized relaxor-type mode in the 1–100 cm⁻¹ low-energy region was found to be important for the BTO ferroelectric phase transition.[41] Derived from the three polar lattice modes, known as Slater, Last, and Axe modes,[43] we expect three well-defined surface phonon polaritons in the surface loss function. Indeed, the HREELS spectrum for the BTO single crystal is characterized by three losses at 190, 465, and 680 cm⁻¹ and their combination and multiple losses as shown in Figure 9a. The frequencies of the surface modes fall in between the

(a)

(b)
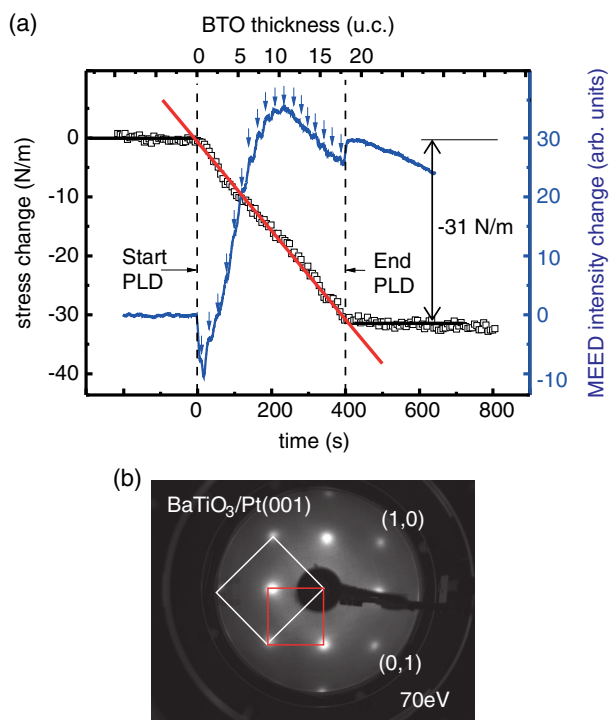
**Figure 8.** a) Stress and MEED measurements during the PLD of 18 unit cells BaTiO$_3$ (BTO) (u.c., 1 u.c. = 4.01 Å) on Pt(001). The solid red line through the stress data indicates a compressive stress of −4.2 GPa, in quantitative agreement with the calculated misfit stress. $T_{sample}$ = 930 K, $p_{O_2}$ = 1 × 10$^{-4}$ mbar. Laser pulse energy: 149 mJ, repetition rate 2 Hz, wavelength: 248 nm. b) LEED pattern at 300 K, after BTO deposition. The white square indicates the (1 × 1)-Pt(001) surface unit cell, the red square the c-(2 × 2) diffraction pattern due to epitaxial BTO growth. Adapted with permission.[14] Copyright 2015, Elsevier (see also ref. [7]).



(a)

(b)

**Figure 9.** a) HREELS spectra for BTO(001) single crystal (black line) and BTO(001) ultrathin films on Pt(001) with thicknesses of 3, 4, 15, and 25 unit cells (u.c.) as marked by open green, open orange, solid blue, and solid red circles, respectively. The inset shows the LEED pattern for the 4 uc-thick BTO(001) film. b) Surface phonon polariton frequencies for the three main modes as functions of film thickness. Dotted blue curves serve as guides for the eye. The black solid line shows the calculated frequency shift based on dielectric theory. The black dashed line includes standing-wave corrections.

corresponding TO and LO bulk frequencies, close to the LO frequency. In bulk BTO, the LO phonons of A$_1$ symmetry have been observed at 190, 475, and 727 cm$^{-1}$,[44] which supports our assignment of the observed energy losses to the three surface phonon polaritons.

The HREEL data for the ultrathin BTO films on Pt(001) in Figure 9a exhibit similar spectra with the same three characteristic energy losses and with a similar intensity distribution. This observation proves immediately the growth of a single (001)-oriented BTO phase. One exception is the thinnest film with an average thickness of three unit cells. The data in Figure 9a indicate that it contains a mode around 870 cm$^{-1}$ in addition to the three BTO(001) surface phonon polaritons. The additional signal may come from areas where the film thickness is reduced and a shifted "monolayer" phase may be formed, which is not discussed here any further. The frequency shift of the three BTO modes as a function of film thickness $d$ is shown in Figure 9b. The low-frequency mode at about 190 cm$^{-1}$ stays constant for all film thicknesses within the experimental error bar. The second mode at 460 cm$^{-1}$ shifts up by about 15 cm$^{-1}$ with decreasing film thickness. Whether the observed shift reversal for the thinnest film is intrinsic or due to the parasitic

phase is still unclear. The strongest response is observed for the high-frequency mode, which corresponds to a vibrational mode that is dominated by oxygen octaeder deformation.[43] This mode shifts up with decreasing thickness by about 80 cm$^{-1}$, as indicated by the dotted blue line, which serves as guide to the eye. Calculations of the HREEL response function based on dielectric theory assuming bulk-like vibrational properties are shown as black lines in Figure 9b and cannot account for the strong upshift. The standing-wave correction (dashed black line), as discussed above for BaO thin films, leads only to small additional upshifts and is also not sufficient to explain the experimentally observed shifts.

Clearly, the phonon properties are modified for ultrathin BTO(001) films on Pt(001) as compared with single-crystal BTO data. The presence of surface stress as determined experimentally, but also the presence of a surface-specific ferroelectric domain structure, may be responsible here.

## 5. Conclusions

To discuss the relation between surface stress and surface phonon shifts further, we will concentrate here on the case of NiO on Ag(001). **Figure 10** shows the relative shift of the FK surface phonon polariton $\Delta\omega/\omega$ as a function of the change in experimentally determined surface stress $\tau - \tau_{13ML}$. As a point of reference we have chosen the surface stress for a thick NiO film of 13 ML because it is the starting point of film relaxation (see Figure 5 and 6). Note that a choice for a thicker film would only lead to a horizontal offset in Figure 10. The figure reports for the first time the correlation between surface stress and surface phonon shift for an oxide thin film. The relative phonon shift can be approximated by a linear dependence on stress change with a slope of $0.013\,\mathrm{m\,N^{-1}}$, as indicated by the red solid line. The vertical offset for $\tau - \tau_{13ML} = 0$ originates from the fact that the frequency is taken relative to NiO bulk, whereas the surface stress change data are relative to a thick film of 13 ML. The "linear" correlation between surface stress and surface phonon shift over a wide range in film thickness from 2 to 13 ML is nontrivial since both quantities, surface stress change and surface phonon frequency, change in a nonlinear way with film thickness, as discussed earlier. For the microscopic phonon modes, we find red shifts for three phonon modes (either at the surface Brillouin zone center or at the boundary) when we compare the strained 4 ML film with unstrained NiO(001), as shown in Figure 7b. As there are no additional data for other film thicknesses available, a direct correlation with the surface stress data is not possible.

In contrast to NiO, we find for the unstrained growth of BaO(001) on Pt(001) only a small frequency shift of the FK surface phonon polariton that is fully explainable by dielectric theory with constant bulk phonon frequencies. It proves that the dipolar modes of ultrathin oxide films with rocksalt structure in the absence of film strain can be well described by dielectric theory, which takes the ultrathin film geometry and the bulk phonon frequencies into account. Therefore, the case of BaO(001) on Pt(001) delivers a justification to discuss the surface phonon polariton shift beyond the dielectric theory for strained NiO ultrathin films in terms of the growth-induced surface stress. Note that we assume no significant stress for the unstrained growth of BaO on Pt(001), for which no surface stress data are available so far.
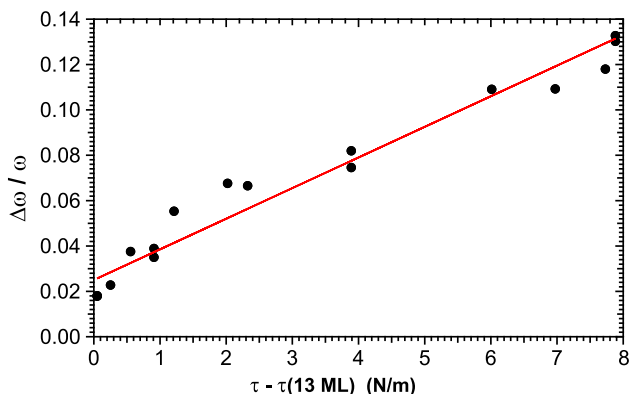
For BTO thin films the situation is more complicated: 1) The BTO surface stress experiments have been conducted during growth at 930 K, whereas the phonon data correspond to 300 K. This difference is particularly important for BTO in view of its structural ferroelectric-to-paraelectric phase transition around 400 K. 2) The ferroelectric domain structure, which is stabilized at the surface for ultrathin films at room temperature, may lead to tetragonal distorted unit cells at the surface.[45] Therefore, the surface stress at room temperature is expected to be significantly modified by the domain structure. 3) The existence of several thin-film polar modes renders a comparison of the shift of only a single phonon mode with surface stress changes being less direct. 4) Note that the low-frequency relaxor-type mode,[41] which is not accessible in the present experiments and which has been reported to be strongly temperature dependent, is likely to couple to stress changes, too. Therefore, the experimentally observed and initially linear down shift from 780 to $730\,\mathrm{cm^{-1}}$ of the high-energy surface phonon polariton cannot be related in a simple way to the linear stress change reported in the same thin-film thickness range.

In general, the interpretation and a detailed understanding of the correlation between surface stress and surface phonon shifts are not straightforward: The surface stress relates to an in-plane force that can be written as the *first* derivative of a potential energy with respect to atomic displacements. The phonon frequency on the other hand is derived from the *second* derivative of the potential energy with respect to atomic displacements. In addition, the displacement pattern relevant for surface stress experiments and optical phonons is not identical. Therefore, a dedicated theoretical approach is required to unravel the experimentally observed correlation between surface stress change and surface phonon shift. To gain deeper insights in this correlation for $BaTiO_3$ thin films, additional experiments on substrates that offer other lattice misfits, as, e.g., Au(001) and Fe(001), would be beneficial as well as a comparison with thin films of other perovskites, as, e.g., $SrTiO_3$.

Clearly, dedicated theoretical investigations are needed. The combined experimental data presented here on surface stress and lattice dynamics in ultrathin oxide thin films of BaO(001), NiO(001), and $BaTiO_3$(001) may initiate such studies and serve as reference data.

## Conflict of Interest

The authors declare no conflict of interest.



**Figure 10.** Relative phonon shift of the FK mode for NiO(001) thin films on Ag(001) as a function of the experimentally determined stress change relative to the stress change for a thick film (13 ML).

[1] D. Schlom, L. Q. Chen, C. B. Eom, K. Rabe, S. Streiffer, J. M. Triscone, *Annu. Rev. Mater. Res.* **2007**, *37*, 589.

[2] D. Tenne, P. Turner, J. Schmidt, M. Biegalski, Y. Li, L. Chen, A. Soukiassian, S. Trolier-McKinstry, D. Schlom, X. Xi, D. Fong, P. Fuoss, J. Eastman, G. Stephenson, C. Thompson, S. Streiffer, *Phys. Rev. Lett.* **2009**, *103*, 177601.

[3] D. Sander, *Rep. Prog. Phys.* **1999**, *62*, 809.

[4] D. Sander, *Curr. Opin. Solid State Mater. Sci.* **2003**, *7*, 51.

[5] D. Sander, *J. Phys.: Condens. Matter* **2004**, *16*, R603.

[6] D. Sander, Z. Tian, J. Kirschner, *Sensors* **2008**, *8*, 4466.

[7] J. Premper, *Ph.D. Thesis*, Martin-Luther-Universität Halle-Wittenberg **2014**.

[8] R. Abermann, *Vacuum* **1990**, *41*, 1279–1282, Selected Proceedings of the 11th International Vacuum Congress (IVC-11) and 7th International Conference on Solid Surfaces (ICSS-7).

[9] R. Koch, *J. Phys.: Condens. Matter* **1994**, *6*, 9519.

[10] H. Ibach, *Surf. Sci. Rep.* **1997**, *29*, 195.

[11] H. Ibach, *Surf. Sci. Rep.* **1999**, *35*, 71.

[12] A. Dhaka, D. Sander, H. Meyerheim, K. Mohseni, E. Soyka, J. Kirschner, W. Adeagbo, G. Fischer, A. Ernst, W. Hergert, *Phys. Rev. B* **2011**, *84*, 195441.

[13] A. Dhaka, *Ph.D. Thesis*, Martin-Luther-Universität Halle-Wittenberg **2012**.

[14] J. Premper, D. Sander, J. Kirschner, *Appl. Surf. Sci.* **2015**, *335*, 44.

[15] J. Premper, D. Sander, J. Kirschner, *Rev. Sci. Instrum.* **2015**, *86*, 33902.

[16] F. Propst, T. Piper, *J. Vac. Sci. Technol.* **1967**, *4*, 53.

[17] H. Ibach, *Phys. Rev. Lett.* **1970**, *24*, 1416.

[18] K. Kostov, M. Gsell, P. Jakob, T. Moritz, W. Widdra, D. Menzel, *Surf. Sci.* **1997**, *394*, L138.

[19] H. Freund, H. Kuhlenbeck, V. Staemmler, *Rep. Prog. Phys.* **1996**, *59*, 283.

[20] M. Finazzi, L. Duo, F. Ciccacci, *Surf. Sci. Rep.* **2007**, *62*, 337.

[21] C. Hagendorf, S. Sachert, B. Bochmann, K. Kostov, W. Widdra, *Phys. Rev. B* **2008**, *77*, 075406.

[22] K. Meinel, M. Huth, H. Beyer, H. Neddermeyer, W. Widdra, *Surf. Sci.* **2014**, *619*, 83.

[23] A. Picone, M. Riva, A. Brambilla, A. Calloni, G. Bussetti, M. Finazzi, F. Ciccacci, L. Duò, *Surf. Sci. Rep.* **2016**, *71*, 32.

[24] J. Kwak, D. Kim, T. Szaidler, C. Peden, J. Szanyi, *Catal. Lett.* **2006**, *111*, 119.

[25] K. Hubbard, D. Schlom, *J. Mater. Res.* **1996**, *11*, 2757.

[26] M. Galtier, A. Montaner, G. Vidal, *J. Phys. Chem. Solids* **1972**, *33*, 2295.

[27] S. Chang, C. Tompson, E. Gürmen, L. Muhlestein, *J. Phys. Chem. Solids* **1975**, *36*, 769.

[28] V. Goian, F. Schumann, W. Widdra, *J. Phys.: Condens. Matter* **2018**, *30*, 095001.

[29] K. Kliewer, R. Fuchs, *Phys. Rev.* **1966**, *150*, 573.

[30] P. Thiry, M. Liehr, J. Pireaux, R. Caudano, *Phys. Rev. B* **1984**, *29*, 4824.

[31] K. Kostov, F. Schumann, S. Polzin, D. Sander, W. Widdra, *Phys. Rev. B* **2016**, *94*, 075438.

[32] K. Kostov, S. Polzin, S. Saha, O. Brovko, V. Stepanyuk, W. Widdra, *Phys. Rev. B* **2013**, *87*, 235416.

[33] S. Großer, C. Hagendorf, H. Neddermeyer, W. Widdra, *Surf. Interface Anal.* **2008**, *40*, 1741.

[34] M. Caffio, B. Cortigiani, G. Rovida, A. Atrei, C. Giovanardi, *J. Phys. Chem. B* **2004**, *108*, 9919.

[35] W. Steurer, F. Allegretti, S. Surnev, G. Barcaro, L. Sementa, F. Negreiros, A. Fortunelli, F. Netzer, *Phys. Rev. B* **2011**, *84*, 115446.

[36] S. Agnoli, T. Orzali, M. Sambi, G. Granozzi, J. Schoiswohl, S. Surnev, F. Netzer, *J. Electron Spectrosc. Relat. Phenom.* **2005**, *144–147*, 465.

[37] G. Dalmai-Imelik, J. Bertolini, J. Rousseau, *Surf. Sci.* **1977**, *63*, 67.

[38] P. Cox, A. Williams, *Surf. Sci.* **1985**, *152–153*, 791.

[39] K. Kostov, S. Polzin, F. Schumann, W. Widdra, *Surf. Sci.* **2016**, *643*, 23.

[40] R. Hammer, K. Meinel, O. Krahn, W. Widdra, *Phys. Rev. B* **2016**, *94*, 195406.

[41] J. Hlinka, T. Ostapchuk, D. Nuzhnyy, J. Petzelt, P. Kuzel, C. Kadlec, P. Vanek, I. Ponomareva, L. Bellaiche, *Phys. Rev. Lett.* **2008**, *101*, 167402.

[42] J. Hwang, T. Kolodiazhnyi, J. Yang, M. Couillard, *Phys. Rev. B* **2010**, *82*, 214109.

[43] J. Axe, *Phys. Rev.* **1967**, *157*, 429.

[44] A. Chaves, R. Katiyar, S. Porto, *Phys. Rev. B* **1974**, *10*, 3522.

[45] A. Höfer, M. Fechner, K. Duncker, M. Hölzer, I. Mertig, W. Widdra, *Phys. Rev. Lett.* **2012**, *108*, 087602.